Surface & Coatings Technology 399 (2020) 126212

Contents lists available at ScienceDirect

Surface & Coatings Technology

journal homepage: www.elsevier.com/locate/surfcoat

Correlation between fracture characteristics and valence electron concentration of sputtered Hf-C-N based thin films

T. Glechner[a,*], S. Lang[a], R. Hahn[a], M. Alfreider[b], V. Moraes[c], D. Primetzhofer[d], J. Ramm[e], S. Kolozsvári[f], D. Kiener[b], H. Riedl[a,c]

[a] Christian Doppler Laboratory for Surface Engineering of high-performance Components, TU Wien, Austria
[b] Department of Materials Science, Montanuniversität Leoben, Austria
[c] Institute of Materials Science and Technology, TU Wien, A-1060 Wien, Austria
[d] Department of Physics and Astronomy, Uppsala University, SE-75120 Uppsala, Sweden
[e] Oerlikon Balzers, Oerlikon Surface Solutions AG, 9496 Balzers, Liechtenstein
[f] Plansee Composite Materials GmbH, D-86983 Lechbruck am See, Germany

ARTICLE INFO

Keywords:
Hf-C-N
Fracture resistance
Non-metal alloying
Valence electron concentration
Thermal stability

ABSTRACT

Hard protective coating materials based on transition metal nitrides and carbides typically suffer from limited fracture tolerance. To further tune these properties non-metal alloying – substituting C with N – has been proven favorable for magnetron sputtered Hf-C-N based thin films. A theoretically predicted increase in valence electron concentration (from 8.0 to 9.0 e/f.u. from Hf—C to Hf—N) through nitrogen alloying lead to an increase in fracture toughness (K_{IC} obtained during in-situ SEM cantilever bending) from 1.89 ± 0.15 to 2.33 ± 0.18 MPa·m$^{1/2}$ for $Hf_{0.43}C_{0.57}$ to $Hf_{0.35}C_{0.30}N_{0.35}$, respectively. The hardness remains close to the superhard regime with values of 37.8 ± 2.1 to 39.9 ± 2.7 GPa for these specific compositions. Already the addition of small amounts of nitrogen, while sputtering a ceramic Hf—C target, leads to a drastic increase of nitrogen on the non-metallic sublattice for fcc single phased structured $HfC_{1-x}N_x$ films, where x = N/(C + N). The here obtained results also provide experimental proof for the correlation between fracture characteristics and valence electron concentration.

1. Introduction

Various challenges in the field of environmental sustainability as well as emission reduction in general are closely linked to the usage of ultra-stable materials. Especially, protective coatings of high-performance components – such as blades or drive train systems in jet engines or steam turbines – depict a key role to achieve further milestones concerning efficiency and operating ranges [1,2]. For these extremely harsh environments, involving highest temperatures accompanied by abrasive and corrosive media, transition metal nitrides (TMN), and carbides (TMC) are highly interesting coating materials due to their excellent thermomechanical properties and chemical inertness [2]. Nevertheless, these ceramic compounds typically lack ductility compared to common metals and metallic alloys [3–5]. Also, the formation of continuous and dense oxide scales at the highest temperatures is a strong limitation for wide usage [7,6].

Among diverse concepts [8], substitutional alloying of the non-metallic sublattice by exchanging C with N atoms – forming carbonitrides – depict an interesting approach to intrinsically tune these coating properties. Through this substitutional exchange, a distinct adaption of the prevalent bonding character and hence valence electron concentration (VEC) is accomplished [9]. This fundamental approach was initially proven for face-centered cubic (fcc) $TiC_{1-x}N_x$ adjusting the VEC to 8.4 e/f.u. exhibiting a hardness maximum due to the population of a particular s band, located between the non-metal p and metal d orbitals, being strongly resistive against shape changes and shearing [10]. While for the hardness a distinct correlation with an ideal VEC for various systems can be made, more or less positive behavior is suggested for the toughness by increasing VEC up to 10 [11–15]. In our previous studies, we could show, that the exchange of about 36% C with N atoms in fcc-structured TaC_y (VEC increasing from 8.24 to 9.36 e/f.u. compared to the binary $TaC_{0.81}$) lead to a fracture toughness increase from 1.8 to 2.9 MPa·m$^{-1/2}$ (while keeping the thin film morphology similar, especially regarding their columnar growth), respectively [4,16]. As already shown in previous studies [17–19], these transition metal carbides and nitrides are strongly effected by structural

* Corresponding author.
E-mail address: thomas.glechner@tuwien.ac.at (T. Glechner).

https://doi.org/10.1016/j.surfcoat.2020.126212
Received 11 March 2020; Received in revised form 2 July 2020; Accepted 16 July 2020
Available online 19 July 2020

defects, such as vacancies, influencing similarly the bonding states. However, a distinct population of structural defects is for sure more challenging compared to non-metal alloying, especially with respect to the deposition process [17]. Furthermore, different theoretical studies using ab initio molecular dynamics [20,21] also predict an increase of the melting temperature of about 200 K for $Hf_{0.53}C_{0.27}N_{0.20}$ compared to pure to Hf—C – suggesting a new highest melting material. Next to these fundamental aspects while exchanging C with N in transition metal carbides, the selection of a proper transition metal is also highly important. Based on their extremely high phase stability and the above-mentioned facts, TaC_y and HfC_y are promising candidates [22]. Especially, the Hafnium based system is encouraging as one oxide is highly stable – in its high-temperature modification (HfO_2, fcc, #SG 225) even up to 3083 K [23,24]. It can be synthesized by reactive cathodic arc evaporation in an Al-Hf-O material system, but it is difficult to stabilize. Studies on Hf-containing thin films [25] and bulk materials [26] suggested high oxidation resistance and hence great potential (even above 1600 °C). However, only a few studies are available for Hf-C-N coatings in general, but also for sputtered deposited coatings. These papers mainly concentrate on the impact of deposition parameters (temperature, bias) on structure, chemical composition as well as tribological performance [27,28].

Therefore, within this study, we combine theoretical Density Functional Theory (DFT) calculations with an experimental validation by magnetron sputtered Hf—C and Hf-C-N thin films. Thereby, we wanted to gain an in-depth understanding of the impact of the non-metallic sublattice occupation (varying nitrogen content) on the thermomechanical properties, especially for fracture tolerance.

2. Experimental procedures

We used two laboratory-scaled magnetron sputtering systems (modified Leybold Heraeus Z400 and AJA Orion 5) having different target to substrate arrangements – a parallel face to face configuration obtaining a target to substrate distance of 50 mm as well as a tilted set-up with a normalized distance of 70 mm – to deposit Hf—C and Hf-C-N thin films. Both deposition systems were equipped with a 3-in. Hf—C compound target (99.6% purity, Plansee Composite Materials GmbH) operated in DC-pulsed mode (pulse frequency 150 kHz, pulse width 2576 ns). The Hf—C coatings were deposited in pure Argon atmosphere (99.999% purity), while Hf-C-N thin films were sputtered reactively in an Argon/Nitrogen gas mixture. All depositions were carried out at a total pressure of 0.4 Pa, as well as a bias potential of −10 V. A base pressure below 10^{-4} Pa was ensured for all deposition runs. We want to emphasize that all coatings were deposited using the same target.

In the tilted setup, a total gas flow of 20 sccm has been used. To obtain different nitrogen concentrations within the Hf-C-N coatings, we varied the amount of nitrogen in the total gas flow ($f_{[N2]}^{norm} = \frac{f_{N_2}}{f_{N_2}+f_{Ar}}$) from 0.0 to 0.15, respectively. The heater temperature was fixed at 600 °C, which corresponds to T_{sub} = 415 ± 15 °C at the substrate surface. The confocally arranged cathode (tilted by 25° to the rotating substrate holder) was powered by an MKS RPG-50 Pulsed DC plasma generator.

For the parallel configuration (bottom to top set-up), all depositions were carried out at a total gas flow of 34.1 sccm. The non-metal sublattice occupation was again varied through the nitrogen to the total gas flow rate from 0.0 to 0.50, respectively. In contrast to the tilted setup, the working gas pressure was not fixed through a pressure valve but adjusted by the gas flow and pumping speed. Therefore, it decreased from 0.393 Pa in pure Argon to 0.376 Pa for $f_{[N2]}^{norm}$ = 0.5. The heater temperature was varied between 300 °C and 500 °C, which corresponds to 250 ± 15 °C and 380 ± 15 °C at the substrate surface, respectively.

Based on the physical limits of the flow controller, our lowest nitrogen to total gas flow ratio ($f_{[N2]}^{norm}$) was 0.05 for both systems. All thin films were deposited on single-crystalline Al_2O_3 platelets (0001-oriented, 10x10x0.53 mm^3), single-crystalline Si stripes (100-oriented, 20x7x0.38 mm^3), and polished austenitic stainless-steel platelets (20x7x0.8 mm^3). Selected coatings were also grown on 0.05 mm thick steel foils, which were dissolved afterward in 20% hydrochloric acid [22]. The residual $Hf_{1-y}C_y$ and $Hf_{1-y-z}C_yN_z$ coating flakes were grounded mechanically to fine-grained powders, which was used for substrate-interference free X-Ray Diffraction (XRD) analysis. Preliminary, to the coating process, the target, and all substrates were sputter-cleaned in a pure Argon atmosphere at a total pressure of 7.0 Pa in the tilted and 1.3 Pa in the face-to-face set up, respectively.

Time-of-flight Elastic Recoil Detection Analysis (ERDA) using a 36 MeV I8+ primary ion beam and detecting recoils at an detection angle of 45° by a segmented gas ionization chamber [29] was performed at the tandem laboratory at Uppsala University to determine the chemical composition of the coatings. Data evaluation is described in more detail in [22]. The structure of all coatings has been analyzed by XRD in Bragg Brentano configuration using a Panalytical Empyrean diffractometer – equipped with a Cu-K_α radiation source operating at 45 kV and 40 mA (wavelength λ = 1.54 Å). Scanning Electron Microscopy (SEM, FEI Quanta 250 FEGSEM operated at 15 kV) was used to scale the coating thicknesses and survey the coating quality in gernal. More detailed analysis on the film morphology was done by Transmission Electron Microscopy (TEM FEI TECNAI G20, an acceleration voltage of 200 kV) – only for selected coatings.

Thermal treatments on sapphire substrates were done in a high-temperature vacuum furnace (Centorr Vacuum Industries Series LF22–2000) up to 1200 °C. The heating rate was 20 $K{\cdot}min^{-1}$ followed by an isothermal annealing time of 10 min and subsequent passively cooling.

Mechanical properties such as Young's modulus and hardness were examined on sapphire substrates by nanoindentation using an Ultra-Micro-Indentation System (UMIS) equipped with a Berkovich diamond tip. For every sample measurement, at least 25 indents with different loads, 3 to 45 mN, were performed and their load-displacement curves were analyzed after Oliver and Pharr [30]. The load range was chosen to identify the ideal range where we have no influence of the substrate and the surface roughness on our obtained values. It should be noted that the indentation depths were below 10% of the film thickness, which is reported to be sufficient to extinguish substrate interference [31]. The Young's modulus was calculated using the Poisson's ratio for $HfC_{1-x}N_x$ obtained by the DFT calculations. In addition, we did not see any clear dependency of the hardness and moduli on the load. All the results presented in this study are averages of hardness and modulus data obtained using loads from 3 to 45 mN (step size varied gradullay from 2 to 0.5 to smaller loads). Residual stresses within the Hf—C and Hf-C-N coatings were investigated by using the modified Stoney Eq. [32]. The curvature of the coated silicon substrates was analyzed by an optical profilometer (Nanovea PS50).

All micro-mechanical tests were done on free-standing cantilevers, which have been prepared by FIB machining. Before FIB-milling (using an FEI Quanta 200 3D DualBeam-FIB), the silicon substrates were etched using an aqueous 40 wt% KOH solution at 70 °C to obtain free-standing film material. After that, the geometry was machined using a beam current of 1.0 nA for coarse milling and 0.5 nA for fine milling at an acceleration voltage of 30 keV. The initial notch was milled with 50 pA. The micromechanical experiments were conducted inside an LEO-1540 FE-SEM/FIB dual-beam workstation with a PI 85 SEM picoindenter mounted. The indenter was equipped with a diamond wedge tip. All experiments were performed in displacement-controlled mode (5 $nm{\cdot}s^{-1}$). The calculation of the fracture toughness was then performed following guidelines given by [33–35]. A load-deflection curve and an image of the fractured cantilever can be found in the supplementary material.

3. Calculational methodology

Density Functional Theory (DFT) calculations were performed with the VASP code (Vienna Ab Initio Simulation Package) [36], using the projector-augmented plane-wave (PAW) pseudopotentials [37]. To gain a deeper insight into the effect of a chosen exchange-correlation (xc) potential, we compared two different standard approximations namely, Local Density Approximation (LDA) [38] and Perdew-Burke-Ernzerhof Generalized Gradient Approximation (GGA-PBE) [39]. We used the fcc, $Fm\bar{3}m$, #SG 225 crystal structure creating a 2 × 2 × 2 supercell with 64 atoms from the conventional 8-a.u. cell. Various $HfC_{1-x}N_x$ compositions were obtained by substituting carbon atoms with nitrogen utilizing the Special Quasi-random Structure (SQS) method [40]. The influence of structural defects was investigated by the systematic removal of either metallic or non-metallic species, also applying the SQS code. The Brillouin zone of the cubic supercell was sampled with 6 × 6 × 6 k-points, and a plane wave cut-off energy of 500 eV was chosen based on convergence tests guaranteeing a total energy accuracy of at least 1 meV/at. Equilibrium lattice parameters and ground-state energies were obtained by relaxing the supercell volumes, shapes, and atomic positions (ISIF = 3 tag in VASP). Elastic constants of the $HfC_{1-x}N_x$ supercells were calculated using the Universal Linear-Independent Coupling Strain (ULICS) method [41].

Polycrystalline bulk and shear modulus (B and G), Poisson ratio (ν), and Young's modulus, E, were calculated applying Hill's average [42] of the Reuss and Voigt bulk moduli (B_R and B_V) and shear moduli (G_R and G_V), respectively.

4. Results and discussion

The angular distribution of metal and non-metal species (due to their diverging atomic masses of Hf = 178.49 u compared to C = 12.01 u) during sputter deposition (e.g. Hf−C) was the main driving force for comparing two different target to substrate alignments [43]. Based on the geometrically differences for these two setups, distinct target currents (0.5 and 0.8 A, respectively), as well as substrate heater temperatures were used to gain similar coating morphologies. The chemical compositions of all coatings ($Hf_{1-y}C_y$ and $Hf_{1-y-z}C_yN_z$) were analyzed by TOF-ERDA. During these measurements, Hafnium (Hf) Carbon (C), and Nitrogen (N), as well as Argon (Ar) and Oxygen (O) were detected. Expected systematic uncertainties in the Hf-C-N system are typically found to be at most 5 to 10% of the detected concentrations for absolute measurements free from standards. Nevertheless, much higher precision is obtained for inter-sample comparison, as performed within this study [43]. For the binary coatings deposited with the parallel and tilted configuration, we obtained $Hf_{0.6}C_{0.4}$ and $Hf_{0.43}C_{0.57}$, respectively. The difference in stoichiometry is related to the angular distribution during sputtering. In Fig. 1, an isothermal section of the ternary Hf-C-N system is presented including the δ-Hf(C, N)$_{1-x}$ (light blue) as well as the α-Hf phase-field as suggested by S. Binder [44] for an experimentally validated isothermal section at 1150 °C (the temperature has no direct relation to the synthesis or growth process and is only based on the limited data set for isothermal sections within the ternary Hf-C-N system). All coatings deposited are plotted in half-filled cubes and open diamonds for the parallel and tilted set-up, respectively. In agreement with a previous study [22], are binary Hf−C compounds most likely off-stoichiometric phases ($Hf_{0.43}C_{0.57}$ and $Hf_{0.6}C_{0.4}$), which is typically observed when using TMC compound targets in Ar atmospheres (in relation to the angular distribution) [45]. Furthermore, already relatively low $f_{[N2]}^{norm}$ results in high nitrogen contents on the non-metallic sublattice, x (x = N/(C + N)). This behavior is also highlighted in Fig. 2, where the non-metallic sublattice occupation is plotted against the nitrogen flow rate and underlines that we were unable to obtain compositions below x = 0.50. The trends are similar for both target configurations and show a big increase in, x, from $f_{[N2]}^{norm}$ = 0 to 0.05, followed by a slight rise for higher nitrogen flow rates (from 0.05 to 0.20). The occupation of nitrogen on the non-metallic sublattice is accompanied not only by a decrease in Carbon but also by a decrease in Hafnium, resulting in Hafnium sub-stoichiometric thin films, deviating from a hypothetical HfC-HfN tie line – see the right border of the δ-Hf (C, N)$_{1-x}$ phase-field indicated in Fig. 1. This behavior is similar to the Ta-C-N system [16], where it is less pronounced. The reduction of the deposition temperature (hence surface mobility of incoming species) enhances this effect further, see open cube (T_{sub} = 250 °C) in Fig. 1, whereby the nitrogen content increases on the cost of the Hf content. The substrate surface temperature also influences the residual stress state within the coatings, increasing the compressive character for decreased surface temperatures from −2.2 GPa to −2.8 GPa for 380 °C and 250 °C, respectively. As the net stress state is influenced by several factors, e.g. temperature and thickness (after R. Abermann [46]), a higher growth rate for T_{sub} = 380 °C (30 nm/min compared to 22 nm/min) most likely dominates the compressive influence. The difference in growth rate is mostly related to the varied nitrogen flow rate ratio for these specific coatings, respectively. Nevertheless, lower surface temperatures, as well as target currents accompanied by higher $f_{[N2]}^{norm}$ might promote the introduction of reactive working gas nitrogen onto the non-metallic sublattice.

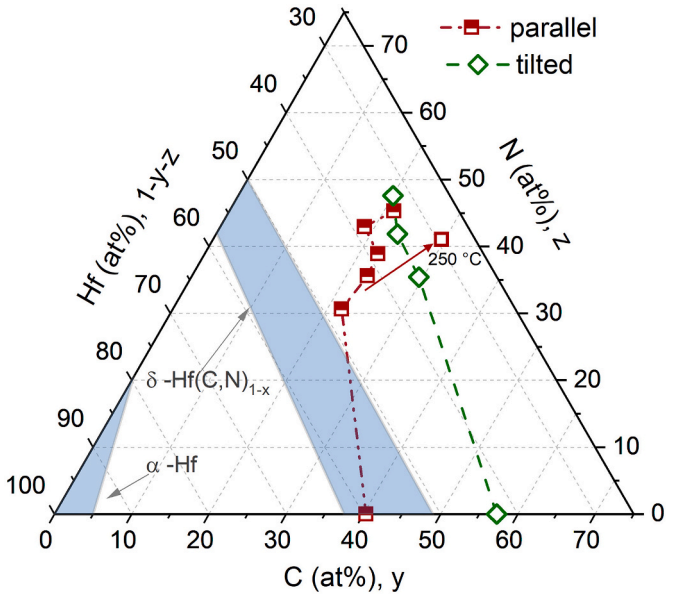

Fig. 1. Isothermal section (1150 °C [44]) of the ternary Hf-C-N system with indicated compositions of the parallel and tilted target configuration obtained by ERDA. Open diamonds refer to the tilted set up (T_{sub} = 415 °C), whereas half-filled cubes indicate coatings obtained from the parallel configuration (T_{sub} = 380 °C). The open cube refers to the composition at a lower substrate temperature (T_{sub} = 250 °C) in the parallel set up with $f_{[N2]}^{norm}$ = 0.05.

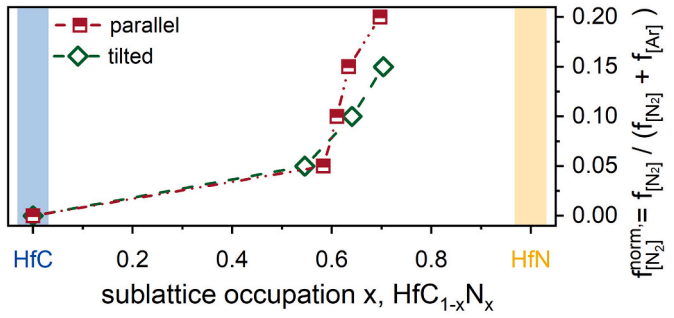

Fig. 2. Influence of the nitrogen to total gas flow ratio $f_{[N2]}^{norm}$ on the nitrogen sublattice occupation x = N/(C + N). The tilted set up is indicated by open diamonds, whereas half-filled squares refer to the parallel configuration.

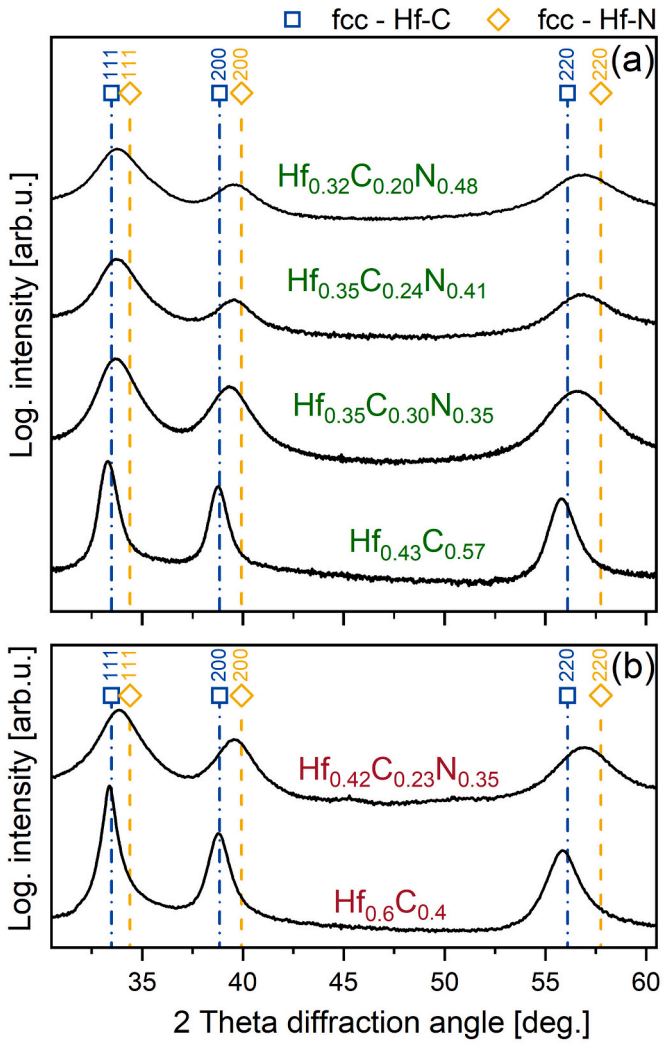

Fig. 3. Structure evolution with increasing nitrogen content for tilted (a) and parallel (b) target to substrate configuration. Spectra are obtained from powdered coatings. The reference fcc-structured Hf–C and Hf–N pattern are taken from [47,48].

Furthermore, the effect of slightly different angular sputter distributions was also obvious in the colors of the coatings. In general, Hf–C coatings appear dark grey up to black, whereas Hf-C-N coatings have a coppery color. Hf-C-N coatings deposited with the face to face arrangement, obtain a color-gradient, from coppery to black to coppery over a distance of 20 mm (substrate size) being centered with respect to the race track. This gradient is contributed to the angular sputter distribution of Hf and C as well as the relatively short substrate to target distance (50 mm). The black regions exhibit about 7 at.% more carbon on the extend of Hf, whereas the nitrogen content remains the same throughout the substrate width. However, no gradient is observed in the coatings deposited using the tilted arrangement. Due to this fact, all further mechanical characterizations and annealing experiments are done on coatings deposited in the tilted setup.

Fig. 3 a and b show the structural evolution with increasing nitrogen content for both experimental set-ups. All coatings, $Hf_{1-y}C_y$ as well as $Hf_{1-y-z}C_yN_z$, exhibit face-centered cubic (fcc) structures. Furthermore, we observe a broadening of the peaks with increasing $f_{[N_2]}^{norm}$ indicating a decrease in crystallite size as well as being a hint for higher defect densities within the columns. The incorporation of nitrogen in the thin films leads to a shift of the 2Θ values to higher angles towards Hf–N, which indicates a smaller lattice parameter [47,48] – visible for pure $Hf_{1-y}C_y$ compared to nitrogen alloyed coatings.

To further evaluate the obtained structural results, we performed TEM investigations shown in Fig. 4 for $Hf_{0.43}C_{0.57}$ (a to c) and $Hf_{0.35}C_{0.24}N_{0.41}$ (d to f), respectively. Films on Si substrate have been prepared for these TEM anlysis. Here a focus is to prove the presence of amorphous phases, as a clear picture about the over stoichiometric Hf–C and Hf-C-N (especially on the non-metal sublattice) compositions is not obvious. Both coatings show a dense columnar growth morphology, while the addition of nitrogen leads to a decreasing column size for the $Hf_{0.35}C_{0.24}N_{0.41}$ coatings – as also seen in the XRD spectra. For $Hf_{0.43}C_{0.57}$ the SAED analysis reavealed distinct spots on a ring-pattern clearly corresponding to fcc structures – see Fig. 4b. These spots get more blurred around the diffraction spots for $Hf_{0.35}C_{0.24}N_{0.41}$ due to smaller diffracting domains (e.g. grains and/or crystallites) – see Fig. 4e. As the dark-field image in Fig. 4e consist out of nice shaped columns, also a highly crystalline state is assumed for the $Hf_{0.35}C_{0.24}N_{0.41}$ coating. The high-resolution image of $Hf_{0.43}C_{0.57}$ (see Fig. 4c) give a detailed insight on the crystal structure and the morphology at the column boundaries, which are marked with white dashed lines. In addition FFT analysis of the marked areas have been conducted to prove the high crystallinity of these areas. The FFT clearly revealed dot-like patterns, suggesting also the crystalline character on this small length scale. For the $Hf_{0.35}C_{0.24}N_{0.41}$ coating, also no obvious amorphous grain boundary phases are visible at a higher resolution (see Fig. 4f). This is an indication, that carbon and nitrogen are sharing the octohetral sites on the non-metal sublattice, and may minor amorphous CNx regions are formed as suggested by further studies [45] on TMC based caotings (reporting access carbon accumalated on grain boundaries in nano-composite morphologies). However, with respect to the access non-metal species in the observed chemistry – and limited experimental proof – we have to admit, that detailed analysis, e.g. using XPS, could draw a more clear picture about the grain boundary morphology (e.g. very thin CN_x interface phases) at this nano-scale level.

The obtained experimental findings on the structural evolution of Hf-C-N were also verified by DFT calculations applying VASP. Fig. 5a shows that the Energy of formation (E_f) lowers with increasing nitrogen content on the non-metallic sublattice, x ($HfC_{1-x}N_x$), suggesting stabilization of Hf–N based structures (using PBE potentials). Compared to calculations for the $TaC_{1-x}N_x$ system [16] the decrease in E_f and hence the driving force to form nitrogen-rich compounds is much stronger for $HfC_{1-x}N_x$. This might be the reason why we observed such a high affinity of incorporating nitrogen during the reactive sputter process. Vacancies (vacancy concentration of 6% on the corresponding sublattice) only slightly influence the phase formation of $HfC_{1-x}N_x$ structures as the defect-free cells are preferred over the full compositional range – please compare open with half-filled and full squares in Fig. 4a, respectively. Nevertheless, Carbon-rich compositions are more prone to non-metal vacancies, whereas HfN prefers metal vacancies. Fig. 5b presents the lattice parameter with respect to the sublattice occupation, x, applying LDA and PBE exchange-correlation potential (xc). The lattice parameter decreases with increasing nitrogen content as it was also observed in the XRD analysis of the thin films. Both potentials result in the same trend but with different absolute values. The calculated lattice parameters are compared with lattice parameters determined by XRD (open diamonds, green) using a LaB_6 standard powder as a reference. Based on simplifications, we used the sublattice occupation x = N/(C + N) for the experimental compositions to compare the calculated with the experimental lattice constants. Nevertheless, the experimental trend matches the PBE lattice parameter quite well. The lattice constants of the XRD references, 4.63 Å [48] and 4.51 Å [47] for HfC and HfN, respectively, are exactly in-between the values obtained by LDA (HfC a_c = 4.58 Å, HfN a_c = 4.46 Å) and PBE (HfC a_c = 4.65 Å, HfN a_c = 4.54 Å).

As already mentioned above, the mechanical properties, especially hardness and elastic modulus, of transition metal carbides and nitrides are strongly influenced by their VEC – obtaining a maximum at VEC of 8.4 e/f.u. This correlation was proven for $TiC_{1-x}N_x$, but still, some

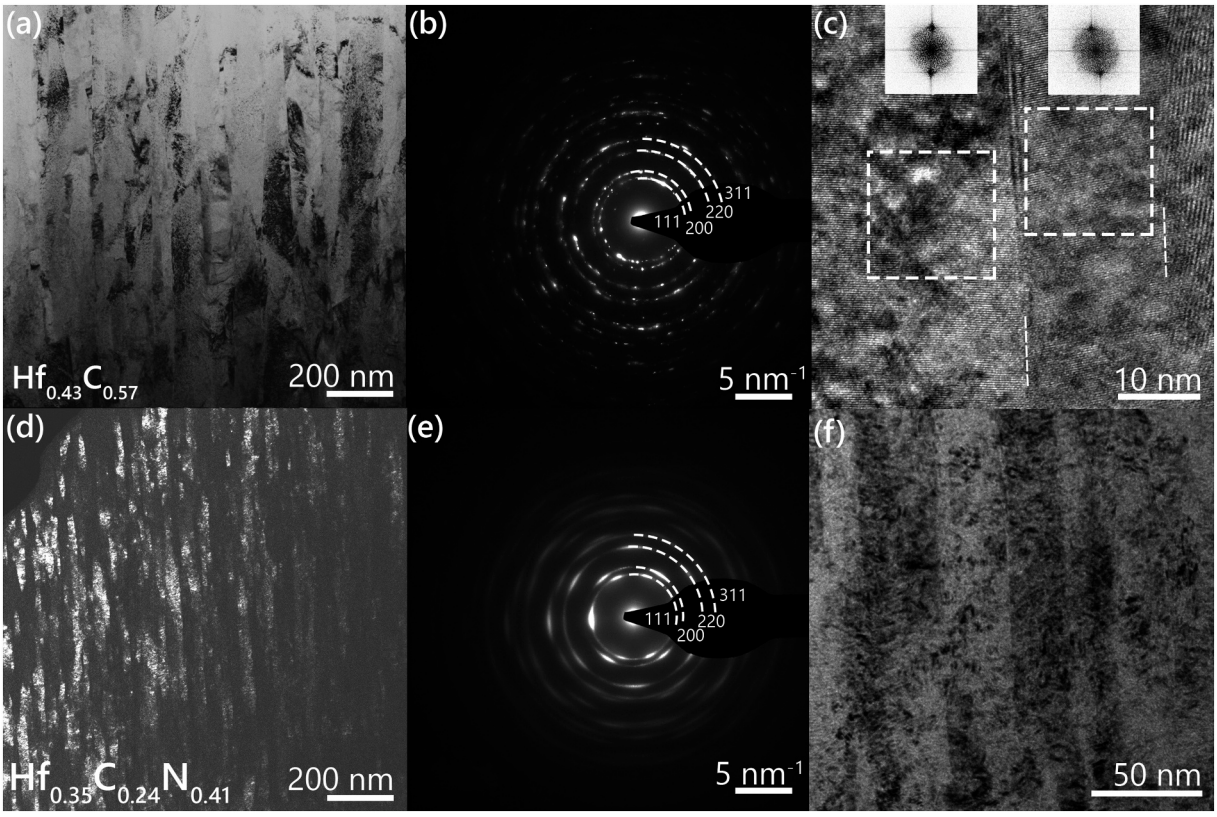

Fig. 4. Cross sectional bright images of $Hf_{0.43}C_{0.57}$ (a) as well as a dark field micrograph of $Hf_{0.35}C_{0.24}N_{0.41}$ (d), respectively (films depsoted on Si substrates). The corresponding SAED analysis to $Hf_{0.43}C_{0.57}$ and $Hf_{0.35}C_{0.24}N_{0.41}$ are given in (b) and (e), respectively. Bright field images with higher resolution (c) and (f) provide a closer look at the column boundaries of the respective coatings. In (c) column boundaries are marked with dashed lines and the insets show the FFTs of the corresponding columns.

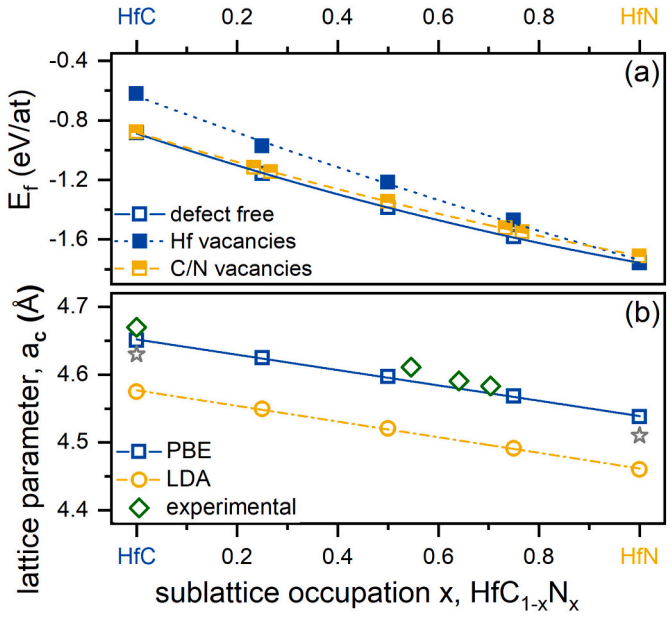

Fig. 5. (a) Trend of the calculated E_f over the nitrogen sublattice occupation, x, for perfect and defected supercells. Defect-free cells possess the lowest E_f and are therefore most preferred. (b) Comparison of the two used xc potentials LDA (open cubes) and PBE (open circles) based on the lattice parameter, a_c. The calculated values are furthermore compared with the experimentally determined ones (open diamonds) from XRD and references (star symbols) [47,48].

questions arise for specific systems with respect to the way how the VEC (e.g. through vacancies) is achieved [13,10,17]. However, a correlation between the fracture tolerance and VEC, and specifically the nitrogen sublattice occupation in transition metal carbide-based materials, is rare. Therefore, this work gives additional information on how the sublattice occupation, hence the VEC, affects the ductility in $HfC_{1-x}N_x$. To develop this correlation, we compared the semi-empirical criteria B/G ratio (Pugh-ratio) [49] as well as Pettifor's Cauchy pressure (C_{12}-C_{44}) [50] with experimentally evaluated fracture characteristics. In addition, Niu et al. proposed recently a universal ductile to brittle criterion ((C_{12}-C_{44})/E) [51]. Fig. 6a gives the Bulk, B (open squares), and Shear modulus, G (half-filled squares) – on which base the Pugh-ratio is calculated – in comparison to literature data (open stars) [13]. The bulk modulus is in good agreement with the endpoints provided by the literature. Furthermore, the increase in B accompanied by a decrease in G suggests higher Pugh-ratios. In Fig. 6b C_{12}-C_{44} and (C_{12}-C_{44})/E are plotted over the VEC, whereby more positive values (above the Pettifor criterion) indicate a more ductile character. The criteria result in the same trend with a small decrease in ductility for VEC = 8.25 e/f.u. (x = 0.25), followed by a subsequent increase with increasing nitrogen content (VEC). However, for all compositions, we are below the Pettifor criterion and hence in the so-called brittle regime.

Comparing the Pugh-ratio of the group IV TM-carbonitride, $HfC_{1-x}N_x$, with the group V TM-carbonitride, $TaC_{1-x}N_x$ [16], with experimentally obtained K_{IC} values emphasizes an almost continuous increase in ductility with increasing VEC, see Fig. 7. Here the fracture toughness, K_{IC}, is plotted on the left y-axis in relation to the VEC and compared with the B/G ratio plotted on the right y-axis for $HfC_{1-x}N_x$ (open squares) and $TaC_{1-x}N_x$ (open circles), respectively. This is in excellent agreement with calculations from Ref. [13] indicating a positive effect on the fracture characteristics for VEC up to 10. All indicated toughness

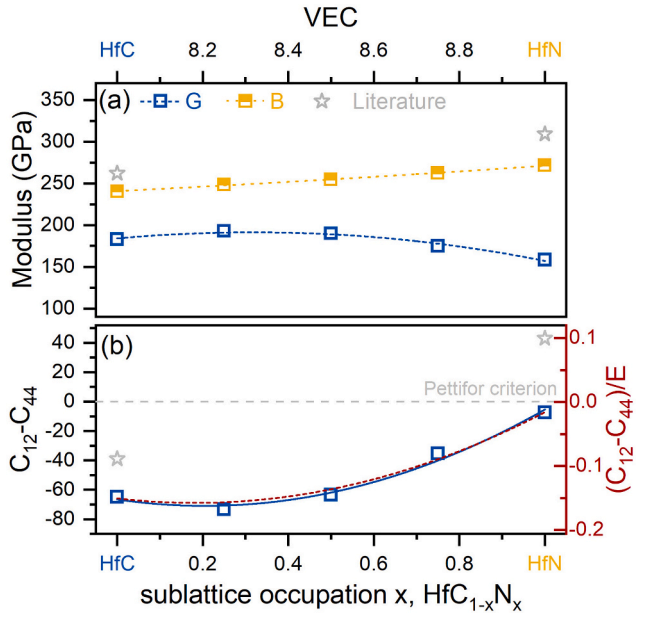

Fig. 6. (a) Bulk modulus (B) and shear modulus (G) as a function of the nitrogen sublattice occupation, x, and hence VEC. (b) Cauchy pressure (C_{12}-C_{44}) and (C_{12}-C_{44})/E in relation to the sublattice occupation with indicated Pettifor criterion – (C_{12}-C_{44}) > 0 is expected to be ductile. Star symbols represent literature [13] values for B and C_{12}-C_{44}.

values, K_{IC}, have been obtained by equal single cantilever beam bending tests (values obtained for at least 5 or more beams). Values for the Ta-C-N system are taken from a previous study [4]. Here the authors want to highlight, that the VEC of all compounds denotes the valence electrons per unit cell as commonly reported in the literature for these compounds [10] only taking into account the carbon substitution with nitrogen in the metal-normalized notation ($HfC_{1-x}N_x$ and $TaC_{1-x}N_x$). Therefore, sub-stoichiometries are more or less neglected within this depiction. For both systems, the introduction of nitrogen increases the fracture toughness following the theoretical predictions. The fracture toughness of the $HfC_{1-x}N_x$ increases from 1.89 ± 0.15 to 2.33 ± 0.18 MPa·$m^{1/2}$ for $Hf_{0.43}C_{0.57}$ and $Hf_{0.35}C_{0.30}N_{0.35}$ respectively.

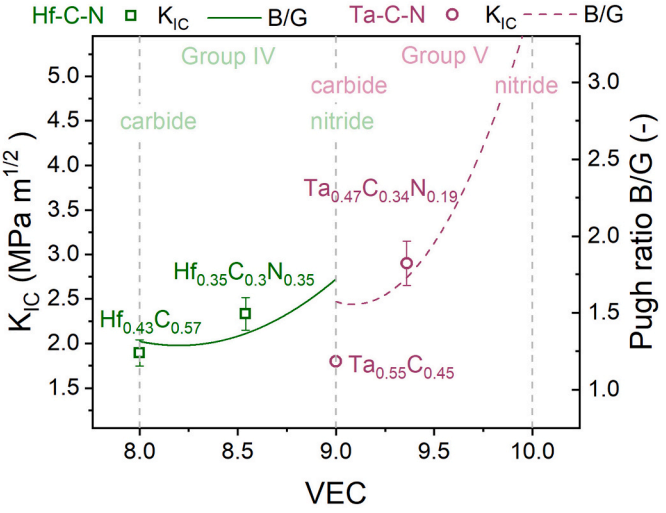

Fig. 7. Empirical criterion for ductility, Pugh ratio (B/G), for Group IV (Hf) and Group V (Ta) TM-Carbonitrides with respect to the VEC [4]. These calculations are compared with experimentally determined K_{IC} values – open square denotes to Hf and open circles to the Ta based systems, respectively. All experimental data analysis were done on Si substrates, with growth temperatures of 415 °C for the Hf-based and 450 °C for the Ta-based films, respectively.

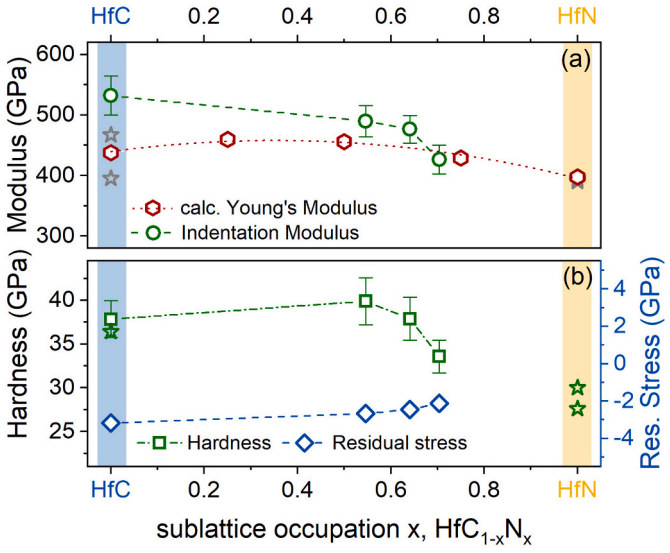

Fig. 8. (a) Experimentally determined Indentation Modulus in relation to the sublattice occupation in comparison to DFT based Young's Modulus values and literature data for HfC and HfN [13,22,51,52] (star symbols). (b) Hardness (open squares) and residual stress (open diamonds) as a function of x (N/(C + N)) in comparison with hardness values from literature [22,51,52] (star symbols). The indentation analysis was performed on Si substrates deposited in the tilted set-up at 415 °C.

The experimentally observed slight increase for $HfC_{1-x}N_x$ also fits the B/G prediction, as the ratio is growing slower with VEC compared to $TaC_{1-x}N_x$. However, the effect of grain size and sub-stoichiometry is neglected here and therefore an absolute comparison is difficult.

To further validate the quality of the theoretically evaluated elastic constants (e.g. B or G), we compare the calculated Young's Modulus with the experimentally determined mechanical properties, especially Indentation Modulus, of the deposited thin films in Fig. 8a. Hardness and indentation modulus were measured on sapphire substrates whereas residual stresses were evaluated on silicon substrates. The predicted Young's Modulus is in good agreement with the measured Indentation Modulus values – see Fig. 8a. For Carbon-rich composition, the slight deviation – also compared to literature data [13,22,52,53] – may be related to the deviations in sub-stoichiometry for the binary $Hf_{1-y}C_y$ system. Nevertheless, the trend follows the already observed results, suggesting moderately reduced Young's modulus with increasing nitrogen contents. In contrast to that, the hardness, see Fig. 8b, starts with a slight increase from 37.8 ± 2.1 to 39.9 ± 2.7 GPa for $Hf_{0.43}C_{0.57}$ to $Hf_{0.35}C_{0.30}N_{0.35}$, respectively. When the nitrogen content is further increased the hardness drops to 33.6 ± 1.9 GPa for $Hf_{0.32}C_{0.20}N_{0.48}$. The residual stress – as plotted in Fig. 8b right y-axis – decreases from −3.2 GPa to −2.1 GPa for x = 0 to x = 0.70, respectively. It follows a different trend than the hardness, which we suggest is due to the bonding nature and not the residual stress, assuming that the residual stress state follows the same trend for the films grown on both sapphire and on silicon substrates. However, we have to mention that: *(i)* the residual stress states may follow a different trend in the samples grown on sapphire (from which hardness data is extracted) from those grown on silicon substrates and *(ii)* even if the stress states were to follow the same trend for the films on both sapphire and silicon, differences in grain sizes and film textures on sapphire and silicon can lead to different trends in hardness of films on sapphire and silicon substrates. Neverthelss, the higher compressive stresses are also in good agreement to the increased deposition rates for Nitrogen poor gas mixture.

As already mentioned, Nitrogen alloying in the Hf—C system is predicted to increase the melting temperature [20]. To investigate the potential change in the mechanical properties of the Hf—C and Hf-C-N coatings due to thermal loading, we performed different annealing tests

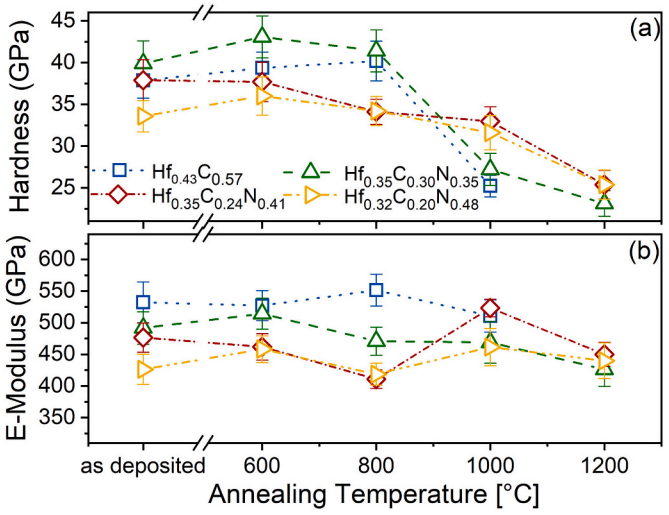

Fig. 9. Hardness (a) and Indentation Modulus (b) of selected coatings after vacuum annealing at 600, 800, 1000, and 1200 °C, respectively. The indentation analysis was performed on films grown (T_{sub} = 415 °C) on sapphire substrates.

and subsequent mechanical characterization, see Fig. 9a and b. We annealed the thin films deposited on sapphire in a vacuum furnace at 600 °C, 800 °C, 1000 °C, and 1200 °C. We observed no visible change in the color of the thin films after annealing up to 800 °C. Beyond this temperature, we observed a change in color towards more greenish or blueish. Furthermore, delamination occurred for the $Hf_{0.43}C_{0.57}$ coating at 1200 °C. However, we assume that in this case, the delamination took place because of the reduced adhesion to the substrate, assumed to be due to high compressive stresses. For all composition tested, the hardness remains almost constant until 800 °C followed by a decrease at higher temperatures. With increasing nitrogen content, the slope for decreasing hardness levels out, and $HfC_{1-x}N_x$ exhibits a higher hardness after annealing. For example, the initial hardness value for $Hf_{0.43}C_{0.57}$ is 37.8 ± 2.1 GPa and after annealing at 1000 °C, it reduces to 25.2 ± 1.3 GPa, whereas for $Hf_{0.35}C_{0.24}N_{0.41}$ the hardness is 37.9 ± 2.4 GPa and after annealing to 1000 °C it settles at 33.0 ± 1.7 GPa, respectively. For all Hf-C-N coatings, the Young's modulus stays approximately constant over the annealing temperature.

5. Conclusion

We investigated the influence of nitrogen alloying on the synthesis, structure, and thermomechanical properties of magnetron sputtered Hf–C thin films. The influence of the non-metallic sublattice occupation x = N/(C + N) – hence the variation of the valance electron concentration – on structural and mechanical properties, was studied both theoretically as well as experimentally. The thin films were deposited by non-reactive and reactive magnetron sputtering from a ceramic Hf–C target. Already at low nitrogen partial pressures, we obtained a high nitrogen content within the coatings, which was even intensified by a lower substrate temperature as well as power density. Therefore, only compositions with x above 0.50 could be deposited. All Hf–C and Hf-C-N coatings exhibit a single-phase fcc structure with dense columnar morphologies. DFT based calculations on the lattice constants – decrease from a_c = 4.65 Å for HfC to a_c = 4.54 Å for HfN – are in excellent agreement with experimental values a_c = 4.67 Å for $Hf_{0.43}C_{0.57}$ and a_c = 4.61 Å for $Hf_{0.35}C_{0.30}N_{0.35}$ (x = 0.54, $HfC_{0.46}N_{0.54}$), respectively. In addition, the predicted elastic constants – B/G ratio as well as Cauchy pressure – also suggest a more ductile character with increasing nitrogen content, implying an increased VEC. This prediction could be also validated experimentally with an increase in fracture toughness from 1.89 ± 0.15 to 2.33 ± 0.18 MPa·$m^{1/2}$ for $Hf_{0.43}C_{0.57}$ to $Hf_{0.35}C_{0.30}N_{0.35}$, respectively. As the VEC ranges between 8.0 e/f.u. to 9.0 e/f.u. for $HfC_{1-x}N_x$ based composition the increase is moderate, as an optimum VEC is suggested slightly below 10. The measured hardness exhibits a maximum of 39.9 ± 2.7 GPa for $Hf_{0.35}C_{0.30}N_{0.35}$. The Young's modulus ranges from 532 to 426 GPa for $Hf_{0.43}C_{0.57}$ and $Hf_{0.32}C_{0.20}N_{0.48}$, respectively. The compressive stress state decreases (−3.2 to −2.1 GPa for x = 0 up to 0.70) with increasing nitrogen content. Nevertheless, we want to mention, that these mechanical enhancements need to be seen in correlation also with morphological changes – which were not clearly observable within this study – and therefore related to the VEC. Furthermore, the non-metal alloying of nitrogen increases the hardness of Hf-C-N coatings after annealing to a maximum of 25.4 ± 1.7 GPa for $Hf_{0.35}C_{0.24}N_{0.41}$ at 1200 °C. In summary, the obtained results indicate the correlation of fracture characteristics and valence electron concentration for transition metal ceramics – such as Hf–C or Hf-C-N. Furthermore, the great potential of Hf-C-N coatings – for well-defined deposition conditions to reach the desired C to N ratios could be validated for its thermomechanical properties.

Supplementary data to this article can be found online at https://doi.org/10.1016/j.surfcoat.2020.126212.

CRediT authorship contribution statement

T. Glechner:Conceptualization, Software, Investigation, Writing - original draft.**S. Lang**:Investigation.**R. Hahn**:Investigation, Writing - review & editing.**M. Alfreider**:Investigation.**V. Moraes**:Investigation.**D. Primetzhofer**:Investigation.**J. Ramm**:Writing - review & editing.**S. Kolozsvári**:Resources.**D. Kiener**:Investigation.**H. Riedl**:Supervision, Conceptualization, Writing - review & editing, Project administration.

Declaration of competing interest

The authors declare that they have no known competing financial interests or personal relationships that could have appeared to influence the work reported in this paper.

Acknowledgments

The financial support by the Austrian Federal Ministry for Digital and Economic Affairs and the National Foundation for Research, Technology, and Development is gratefully acknowledged (Christian Doppler Laboratory “Surface Engineering of high-performance Components”). We also thank for the financial support of Plansee SE, Plansee Composite Materials GmbH, and Oerlikon Balzers, Oerlikon Surface Solutions AG. In addition, we want to thank the X-ray center (XRC) of TU Wien for beam time as well as the electron microscopy center - USTEM TU Wien - for using the SEM and TEM facilities. The computational results presented have been achieved using the Vienna Scientific Cluster (VSC). The authors acknowledge the TU Wien Bibliothek for financial support through its Open Access Funding Program.

References

[1] W.G. Fahrenholtz, G.E. Hilmas, Oxidation of ultra-high temperature transition metal diboride ceramics, Int. Mater. Rev. 57 (2012) 61–72.
[2] W.G. Fahrenholtz, E.J. Wuchina, W.E. Lee, Y. Zhou, Ultra-high Temperature Ceramics: Materials for Extreme Environment Applications, John Wiley & Sons, 2014.
[3] S. Kiani, J. Yang, S. Kodambaka, Nanomechanics of refractory transition-metal carbides: a path to discovering plasticity in hard ceramics, J. Am. Ceram. Soc. 98 (2015) 2313–2323.
[4] T. Glechner, R. Hahn, T. Wojcik, D. Holec, S. Kolozsvári, H. Zaid, S. Kodambaka, P.H. Mayrhofer, H. Riedl, Assessment of ductile character in superhard Ta-C-N thin films, ta Mater Ac (2019).
[5] H. Kindlund, D.G. Sangiovanni, I. Petrov, J.E. Greene, L. Hultman, A review of the intrinsic ductility and toughness of hard transition-metal nitride alloy thin films,

Thin Solid Films 688 (2019) 137479.
[6] R. Hollerweger, H. Riedl, M. Arndt, S. Kolozsvari, S. Primig, P.H. Mayrhofer, Guidelines for increasing the oxidation resistance of Ti-Al-N based coatings, Thin Solid Films 688 (2019) 137290.
[7] D.E. Hajas, M. to Baben, B. Hallstedt, R. Iskandar, J. Mayer, J.M. Schneider, Oxidation of Cr2AlC coatings in the temperature range of 1230 to 1410°C, Surf. Coat. Technol. 206 (2011) 591–598.
[8] P.H. Mayrhofer, R. Rachbauer, D. Holec, F. Rovere, J.M. Schneider, 4.14 - protective transition metal nitride coatings, in: V.K. Sarin, L. Llanes, D. Mari, C.E. Nebel (Eds.), Comprehensive Materials Processing, Elsevier, Oxford, 2014, pp. 355–388.
[9] H. Holleck, Material selection for hard coatings, J. Vac. Sci. Technol. A 4 (1986) 2661–2669.
[10] S.-H. Jhi, J. Ihm, S.G. Louie, M.L. Cohen, Electronic mechanism of hardness enhancement in transition-metal carbonitrides, Nature 399 (1999) 132.
[11] D.G. Sangiovanni, L. Hultman, V. Chirita, Supertoughening in B1 transition metal nitride alloys by increased valence electron concentration, Acta Mater. 59 (2011) 2121–2134.
[12] D.G. Sangiovanni, V. Chirita, L. Hultman, Electronic mechanism for toughness enhancement in TixM1-xN (M = Mo and W), Phys. Rev. B: Condens. Matter Mater. Phys. 81 (2010) 104107.
[13] K. Balasubramanian, S.V. Khare, D. Gall, Valence electron concentration as an indicator for mechanical properties in rocksalt structure nitrides, carbides and carbonitrides, Acta Mater. 152 (2018) 175–185.
[14] X.-X. Yu, G.B. Thompson, C.R. Weinberger, Influence of carbon vacancy formation on the elastic constants and hardening mechanisms in transition metal carbides, J. Eur. Ceram. Soc. 35 (2015) 95–103.
[15] N. Koutná, D. Holec, O. Svoboda, F.F. Klimashin, P.H. Mayrhofer, Point defects stabilise cubic Mo-N and Ta-N, J. Phys. D. Appl. Phys. 49 (2016) 375303.
[16] T. Glechner, P.H. Mayrhofer, D. Holec, S. Fritze, E. Lewin, V. Paneta, D. Primetzhofer, S. Kolozsvári, H. Riedl, Tuning structure and mechanical properties of Ta-C coatings by N-alloying and vacancy population, Sci. Rep. 8 (2018) 17669.
[17] H. Riedl, T. Glechner, T. Wojcik, N. Koutná, S. Kolozsvári, V. Paneta, D. Holec, D. Primetzhofer, P.H. Mayrhofer, Influence of carbon deficiency on phase formation and thermal stability of super-hard TaCy thin films, Scr. Mater. 149 (2018/5) 150–154.
[18] M. Raza, D. Cornil, J. Cornil, S. Lucas, R. Snyders, S. Konstantinidis, Oxygen vacancy stabilized zirconia (OVSZ); a joint experimental and theoretical study, Scr. Mater. 124 (2016) 26–29.
[19] M. to Baben, M. Hans, D. Primetzhofer, S. Evertz, H. Ruess, J.M. Schneider, Unprecedented thermal stability of inherently metastable titanium aluminum nitride by point defect engineering, Materials Research Letters 5 (2017) 158–169.
[20] Q.-J. Hong, A. van de Walle, Prediction of the material with highest known melting point from ab initio molecular dynamics calculations, Phys. Rev. B Condens. Matter 92 (2015) 020104.
[21] Q.-J. Hong, Methods for melting temperature calculation, phd, California Institute of Technology, http://resolver.caltech.edu/CaltechTHESIS:11092014-074023936, (2015) , Accessed date: 9 August 2016.
[22] H. Lasfargues, T. Glechner, C.M. Koller, V. Paneta, D. Primetzhofer, S. Kolozsvári, D. Holec, H. Riedl, P.H. Mayrhofer, Non-reactively sputtered ultra-high temperature Hf-C and Ta-C coatings, Surf. Coat. Technol. 309 (2017) 436–444.
[23] D.T. Livey, The high temperature stability of oxides and sulphides, Journal of the Less Common Metals 1 (1959) 145–151.
[24] P. Zeman, Š. Zuzjaková, P. Mareš, R. Čerstvý, M. Zhang, J. Jiang, E.I. Meletis, J. Vlček, Superior high-temperature oxidation resistance of magnetron sputtered Hf–B–Si–C–N film, Ceram. Int. 42 (2016) 4853–4859.
[25] Y. Shen, J.C. Jiang, P. Zeman, V. Šímová, J. Vlček, E.I. Meletis, Microstructure evolution in amorphous Hf-B-Si-C-N high temperature resistant coatings after annealing to 1500 °C in air, Sci. Rep. 9 (2019) 3603.
[26] W.G. Fahrenholtz, G.E. Hilmas, Ultra-high temperature ceramics: materials for extreme environments, Scr. Mater. 129 (2017) 94–99.
[27] W.F. Piedrahita, W. Aperador, J.C. Caicedo, P. Prieto, Evolution of physical properties in hafnium carbonitride thin films, J. Alloys Compd. 690 (2017) 485–496.
[28] W. Li, D. Ming-hui, Z. Hong-sen, Z. Bin, Study on HfC N coatings deposited on biomedical AISI 316L by radio-frequency magnetron sputtering, J. Alloys Compd. 730 (2018) 219–227, https://doi.org/10.1016/j.jallcom.2017.09.289.
[29] P. Ström, P. Petersson, M. Rubel, G. Possnert, A combined segmented anode gas ionization chamber and time-of-flight detector for heavy ion elastic recoil detection analysis, Rev. Sci. Instrum. 87 (2016) 103303.
[30] W.C. Oliver, G.M. Pharr, An improved technique for determining hardness and elastic modulus using load and displacement sensing indentation experiments, J. Mater. Res. 7 (1992) 1564–1583.
[31] R. Saha, W.D. Nix, Effects of the substrate on the determination of thin film mechanical properties by nanoindentation, Acta Mater. 50 (2002) 23–38.
[32] G.C.A.M. Janssen, M.M. Abdalla, F. van Keulen, B.R. Pujada, B. van Venrooy, Celebrating the 100th anniversary of the Stoney equation for film stress: developments from polycrystalline steel strips to single crystal silicon wafers, Thin Solid Films 517 (2009) 1858–1867.
[33] K. Matoy, H. Schönherr, T. Detzel, T. Schöberl, R. Pippan, C. Motz, G. Dehm, A comparative micro-cantilever study of the mechanical behavior of silicon based passivation films, Thin Solid Films 518 (2009) 247–256.
[34] S. Brinckmann, C. Kirchlechner, G. Dehm, Stress intensity factor dependence on anisotropy and geometry during micro-fracture experiments, Scr. Mater. 127 (2017) 76–78.
[35] S. Brinckmann, K. Matoy, C. Kirchlechner, G. Dehm, On the influence of microcantilever pre-crack geometries on the apparent fracture toughness of brittle materials, Acta Mater. 136 (2017) 281–287.
[36] G. Kresse, J. Furthmüller, Efficient iterative schemes for ab initio total-energy calculations using a plane-wave basis set, Phys. Rev. B Condens. Matter 54 (1996) 11169–11186.
[37] G. Kresse, D. Joubert, From ultrasoft pseudopotentials to the projector augmented-wave method, Phys. Rev. B Condens. Matter 59 (1999) 1758–1775.
[38] W. Kohn, L.J. Sham, Self-consistent equations including exchange and correlation effects, Phys. Rev. 140 (1965) A1133–A1138.
[39] J.P. Perdew, K. Burke, M. Ernzerhof, Generalized gradient approximation made simple, Phys. Rev. Lett. 77 (1996) 3865–3868.
[40] S. Wei, L.G. Ferreira, J.E. Bernard, A. Zunger, Electronic properties of random alloys: special quasirandom structures, Phys. Rev. B Condens. Matter 42 (1990) 9622–9649.
[41] R. Yu, J. Zhu, H.Q. Ye, Calculations of single-crystal elastic constants made simple, Comput. Phys. Commun. 181 (2010) 671–675.
[42] R. Hill, The elastic behaviour of a crystalline aggregate, Proc. Phys. Soc. A. 65 (1952) 349.
[43] J. Neidhardt, S. Mráz, J.M. Schneider, E. Strub, W. Bohne, B. Liedke, W. Möller, C. Mitterer, Experiment and simulation of the compositional evolution of Ti–B thin films deposited by sputtering of a compound target, J. Appl. Phys. 104 (2008) 063304.
[44] S. Binder, W. Lengauer, P. Ettmayer, J. Bauer, J. Debuigne, M. Bohn, Phase equilibria in the systems Ti-C-N, Zr-C-N and Hf-C-N, J. Alloys Compd. 217 (1995) 128–136.
[45] U. Jansson, E. Lewin, Sputter deposition of transition-metal carbide films — a critical review from a chemical perspective, Thin Solid Films 536 (2013) 1–24.
[46] R. Abermann, Measurements of the intrinsic stress in thin metal films, Vacuum 41 (1990) 1279–1282.
[47] International Center of Diffraction Data, Powder Diffraction File 04-002-0653, (2019).
[48] International Center of Diffraction Data, Powder Diffraction File 04-004-8343, (2019).
[49] S.F. Pugh, XCII. Relations between the elastic moduli and the plastic properties of polycrystalline pure metals, The London, Edinburgh, and Dublin Philosophical Magazine and Journal of Science 45 (1954) 823–843.
[50] D.G. Pettifor, Theoretical predictions of structure and related properties of intermetallics, Mater. Sci. Technol. 8 (1992) 345–349.
[51] H. Niu, X.-Q. Chen, P. Liu, W. Xing, X. Cheng, D. Li, Y. Li, Extra-electron induced covalent strengthening and generalization of intrinsic ductile-to-brittle criterion, Sci. Rep. 2 (2012) 718.
[52] C. Hu, X. Zhang, Z. Gu, H. Huang, S. Zhang, X. Fan, W. Zhang, Q. Wei, W. Zheng, Negative effect of vacancies on cubic symmetry, hardness and conductivity in hafnium nitride films, Scr. Mater. 108 (2015) 141–146.
[53] M.M.S. Villamayor, J. Keraudy, T. Shimizu, R.P.B. Viloan, R. Boyd, D. Lundin, J.E. Greene, I. Petrov, U. Helmersson, Low temperature (T s / T m \textless 0.1) epitaxial growth of HfN/MgO(001) via reactive HiPIMS with metal-ion synchronized substrate bias, J. Vac. Sci. Technol. A 36 (2018) 061511.